Manufacturing Letters 39 (2024) 1–5

Contents lists available at ScienceDirect

Manufacturing Letters

journal homepage: www.elsevier.com/locate/mfglet

Letters

# Minimum cost, stability constrained preform optimization for hybrid manufacturing ☆

Gregory Corson [a], Christopher Tyler [b], Jake Dvorak [a], Tony Schmitz [a,b,*]

[a] University of Tennessee, Mechanical, Aerospace, and Biomedical Engineering, Knoxville, TN, USA
[b] Oak Ridge National Laboratory, Manufacturing Science Division, Oak Ridge, TN, USA

ARTICLE INFO

*Article history:*
Received 10 May 2023
Received in revised form 18 September 2023
Accepted 30 October 2023
Available online 8 November 2023

*Keywords:*
Additive manufacturing
Milling
Optimization
Chatter
Cost

ABSTRACT

This paper describes a new mathematical framework for optimum preform design in hybrid manufacturing, where additive manufacturing is combined with machining. The framework minimizes the combined cost for deposition and machining, while respecting the constraint imposed by machining stability (i.e., machining parameters that produce chatter are rejected). A case study is presented where a thin wall design is parameterized to describe the overbuilt deposition geometry. A grid of candidate solutions is selected to calculate cost and the stability limit considering both the part and tool dynamics. The minimum cost option is deposited and machined to demonstrate the approach.



## 1. Introduction

Topology optimization is a popular approach for distributing material within a pre-selected spatial design domain. Typically, the domain is discretized into a grid and material is assigned to each element (filled) or not (void). For example, the solid isotropic material with penalization (SIMP) method provides an iterative optimization framework to identify the material distribution that minimizes global compliance (i.e., maximizes global stiffness) based on anticipated static loads [1–3]. Constraints may be applied based on maximum stress or lowest eigenvalue, for example, to accept or reject candidate designs [4–6].

In hybrid manufacturing, additive manufacturing processes are used for layer-by-layer material deposition and machining is used to remove material from the printed preform to obtain the desired surface finish and dimensional tolerances. In topology optimization for hybrid manufacturing, the compliance minimization leads to near net shape preforms where material is only added at the locations required to meet the design constraints. While this reduces the amount of preform material, the corresponding dynamic stiffness can be low. This frequency dependent, dynamic stiffness is described using the frequency response function, or FRF, measured or predicted at one or more locations on the preform.

The challenge associated with low dynamic stiffness performs is that the milling stability is compromised. The result is chatter, a self-excited vibration that leads to poor surface finish, large forces and vibrations, and potential preform and/or tool damage. Modeling efforts have demonstrated that stable spindle speed-depth of cut combinations may be selected to avoid chatter, but these depend on the FRF and force model, which relates the cutting force components to the commanded chip width and thickness for the selected workpiece material and cutting edge geometry [7]. To avoid chatter in the presence of low dynamic stiffness, the axial and radial depths of cut must be small which, in turn, increases the machining time. For this reason, the potential cost savings associated with reduced material use are lost due to the high machining time. Prior work to address thin wall preform design includes: selection of stock thickness, stock shape, and tool axis orientation for increased stability in five-axis milling [8]; and the addition of stiffening features that react the dynamic machining forces, but are removed from the preform during machining [9].

☆ Notice: This manuscript has been authored by UT-Battelle, LLC, under contract DE-AC05-00OR22725 with the US Department of Energy (DOE). The US government retains and the publisher, by accepting the article for publication, acknowledges that the US government retains a nonexclusive, paid-up, irrevocable, worldwide license to publish or reproduce the published form of this manuscript, or allow others to do so, for US government purposes. DOE will provide public access to these results of federally sponsored research in accordance with the DOE Public Access Plan (https://energy.gov/downloads/doe-public-access-plan).

* Corresponding author.
*E-mail address:* tony.schmitz@utk.edu (T. Schmitz).

https://doi.org/10.1016/j.mfglet.2023.10.004

The constrained cost minimization is described in Eq. 1, where $C$ is the hybrid manufacturing cost, $b$ is the axial depth of cut, and $b_{\text{lim}}$ is the limiting axial depth to avoid chatter for a selected spindle speed, $\Omega$, and radial depth. Equation 1 specifies that cost is to be minimized (min $C$) subject to (*s.t.*) the selection of stable axial depths ($b < b_{\text{lim}}$).

$$\min\ C\ s.t. b < b_{\text{lim}} \tag{1}$$

To realize minimum cost with stable milling, the following steps were completed: a) parameterize the flexible preform design for a discretized range of overbuilt material on the intended geometry; b) select a preform design using any structural optimization routine and calculate the deposition cost; c) use the tool-holder-spindle and preform FRFs and cutting force model to identify chatter-free milling parameters and calculate the machining cost for each design; and d) select the preform design that provides the minimum hybrid manufacturing cost, which includes both the deposition and machining contributions. Note that this framework can also accommodate surface location error, SLE, caused by forced vibrations during stable machining by selecting $(\Omega, b)$ pairs with SLE less than a user-specified limit [7]. The paper is organized to describe each step. An experimental example is provided to demonstrate the approach.

## 2. Preform design selection

The intended thin wall geometry had a 5 mm thickness, 75 mm height, and 100 mm width; see Fig. 1. The integrated base approximated fixed-free boundary conditions when clamped in a vise. The preforms were additively manufactured by fused filament fabrication (FFF) using ULTEM™ 9085 resin, a high-performance polyetherimide (PEI) thermoplastic popular in aerospace applications due to its high strength-to-weight ratio and chemical resistance. The wall front and back were overbuilt to increase stiffness (blue material in Fig. 1) and machined to the final uniform thickness.

For this initial study, the overbuild geometry was parameterized using two variables, although this is not required for the new framework. The additional thickness at the top, $t_1$, was varied from 1 mm to 10 mm in 1 mm increments. The additional thickness at the base, $t_2$, was varied from $t_1$ to 10 mm, also in 1 mm increments. This provided a vertical boundary when $t_1$ and $t_2$ were equal, or a sloping boundary when $t_2$ was greater than $t_1$ (shown).

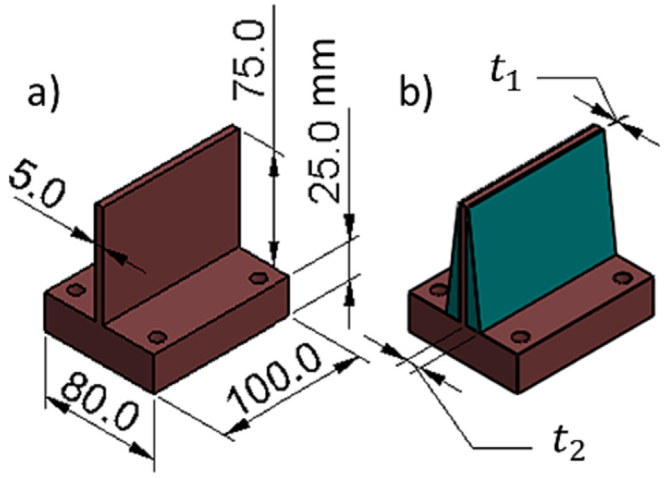


**Fig. 1.** (a) thin wall geometry and (b) parameterized preform design.

## 3. Milling parameter selection

In order to program the CNC tool paths for removal of the overbuilt material, a milling stability analysis was conducted to select stable spindle speed-axial depths combinations. The average force angle solution was applied here [7], which projects the cutting force onto the tool-workpiece FRFs in the feed, $x$, and $y$ directions and these results onto the surface normal direction, which is defined as the average of the start, $\phi_s$, and exit, $\phi_e$, angles of the endmill for a given radial depth and milling direction. See Eq. 2, where $K_s$ is the specific cutting force, $Re[G_{\text{orient}}]$ is the negative real part of the tool-workpiece FRFs oriented in the surface normal direction, and $N_t^*$ is the average number of teeth engaged in the cut; see Eq. 3, where $N_t$ is the number of teeth on the endmill. In Eq. 4, $f_c$ is the chatter frequency (should it occur), $\Omega$ is spindle speed, $N$ is the integer number of waves between teeth ($N$ = 0, 1, 2, ...), and $\varepsilon$ is the fractional phase between the waves; see Eq. 5. A stability map is constructed by plotting $b_{\text{lim}}$ vs. $\Omega$, where the spindle speed vector is determined for each $N$ value by solving Eq. 4 using the range of chatter frequencies from the negative real part of the oriented FRF and the phase is determined using Eq. 5.

$$b_{\text{lim}} = \frac{-1}{2K_s Re[G_{\text{orient}}]N_t^*} \tag{2}$$

$$N_t^* = \frac{\phi_e - \phi_s}{\frac{2\pi}{N_t}} \tag{3}$$

$$\frac{f_c}{\Omega N_t} = N + \frac{\varepsilon}{2\pi} \tag{4}$$

$$\varepsilon = 2\pi - 2\tan^{-1}\left(\frac{Re[G_{\text{orient}}]}{Im[G_{\text{orient}}]}\right) \tag{5}$$

The tool-holder-spindle FRFs in the $x$ and $y$ directions were measured by impact testing, where a low-mass accelerometer (PCB 352C23) recorded the response due to an instrumented hammer impact (PCB 086C03) at the tool's free end. The 12.7 mm diameter endmill had three teeth and a corner radius of 0.381 mm. It was held in a CAT40 taper, ER32 collet with an extension length of 86.5 mm from the holder face. The in-process workpiece (IPW) FRFs in the $y$ direction were simulated using Abaqus™, a commercial finite element (FE) package, where the ULTEM™ 9085 was modeled as isotropic with a density of 1270 kg/m$^3$, an elastic modulus of 2.52 GPa, and Poisson's ratio of 0.39. The wall and overbuilt geometry were modeled separately and meshed with linear hexahedral elements (C3D8R). This enabled the overbuilt material to be incrementally removed in the $z$ direction during machining. For each simulation, the first five mode shapes were calculated and the mass normalized mode shapes were saved. The preform FRF, $\frac{Y}{F}(\omega)$, at each FE node was then calculated using Eq. 6, where $r$ is the mode number, $\omega$ is the frequency, $\phi_r$ is the mass normalized mode shape, $\omega_{n,r}$ is the natural frequency, and $\xi_r$ is the modal damping ratio. For accurate modal damping ratios, a preform of the final geometry wall was deposited and impact testing was performed (PCB 086E80 hammer). The modal damping ratios were found to be {0.024, 0.017, 0.011, 0.011, 0.011} using a peak picking procedure [7]. These values were used to define the mode-dependent, non-dimensional damping ratios in the wall FE model.

$$\frac{Y}{F}(\omega) = \sum_{r=1}^{5} \frac{\phi_r \phi_r^T}{\omega_{n,r}^2 - \omega^2 + i\xi_r\omega_{n,r}^2} \tag{6}$$

The mechanistic force model coefficients (see Eqs. 7 and 8) were determined using a linear regression to the mean force in the $x$ (feed) and $y$ directions over a range of feed per tooth values, $f_t$, from

50 μm to 100 μm [7]. In Eqs. 7 and 8, $k_{tc}$ and $k_{te}$ are the cutting and edge coefficients in the tangential direction, $k_{nc}$ and $k_{ne}$ are the normal direction coefficients, $b$ is the axial depth, $\phi$ is the tool rotation angle, and $F_{x,y}$ are the measured forces. The forces were measured using a Kistler 9257B dynamometer.

$$F_x = k_{tc} b f_t \sin(\phi) \cos(\phi) + k_{te} b \cos(\phi) + k_{nc} b f_t \sin^2(\phi) + k_{ne} b \times \sin(\phi) \quad (7)$$

$$F_y = k_{tc} b_{ft} \sin^2(\phi) + k_{te} b \sin(\phi) - k_{nc} b f_t \sin(\phi) \cos(\phi) - k_{ne} b \times \cos(\phi) \quad (8)$$

The $K_s$ and force angle, $\beta$, values were then calculated using Eqs. 9 and 10. The results for the selected tool and ULTEM™ 9085 were $k_{tc}$ = 152 N/mm$^2$, $k_{te}$ = 0.002 N/mm, $k_{nc}$ = 10.5 N/mm$^2$, $k_{ne}$ = 0.002-N/mm, $K_s$ = 152.4 N/mm2, and $\beta$ = 86 deg.

$$K_s = \sqrt{k_{tc}^2 + k_{nc}^2} \quad (9)$$

$$\beta = \tan^{-1}\left(\frac{k_{tc}}{k_{nc}}\right) \quad (10)$$

Stability maps were calculated at each FE node for each row as the overbuilt geometry was removed from top to bottom. The stability maps used the predicted FRFs at the top of the overbuilt material, measured tool tip FRFs, cutting force coefficients, and radial depth of cut (where the preform was machined to its finish dimension in a single pass). The stability maps from all nodes were then superimposed to identify the minimum value at each spindle speed and construct a "global" stability map, which ensured stable conditions for the entire machining operation. Based on the global stability map, the final machining conditions were selected. The spindle speed for the maximum stable material removal rate (MRR) was first chosen. Then, the axial depth of cut was chosen as the average depth of cut from the maximum MRR point and the critical stability limit, $b_{lim,crit}$ (i.e., the minimum value from the stability boundary); see Fig. 2, where this approach was selected to accommodate uncertainties in the stability model and inputs.

## 4. Hybrid manufacturing cost

The hybrid manufacturing, HM, cost is shown in Eq. 11, where $C_{HM}$, is the sum of the additive manufacturing (AM) cost, $C_{AM}$, and machining (M) cost, $C_M$.

$$C_{HM} = C_{AM} + C_M \quad (11)$$

The AM cost is calculated using Eqs. 12 to 14. In Eq. 12, $v_s$ is the AM slicer deposition volume (GrabCAD™), $r_m$ is the material cost per unit volume, $r_{t,AM}$ is the machine and operator cost per unit time, $\bar{p}_{AM}$ is the average electrical power consumption, $r_e$ is the electrical power cost per unit time, $t_{AM}$ is the deposition time, and $C_{fix,AM}$ is the fixed cost. In Eq. 13, a linear regression was completed to model the sliced preform volume as a function of the computer aided design (CAD) part volume, $v_{CAD}$. In Eq. 14, a linear regression was used to model the AM time as a function of the preform volume for a selected machine.

$$C_{AM} = v_s r_m + \left(r_{t,AM} + \bar{p}_{AM} r_e\right) t_{AM} + C_{fix,AM} \quad (12)$$

$$v_S = 0.908\, v_{CAD} + 5 \times 10^{-6} \quad (13)$$

$$t_{AM} = 14719\, v_s + 1.4301 \quad (14)$$

The machining process costs were modeled using Eqs. 15 to 21. In Eq. 15, $r_{t,M}$ is the cost per unit time for the machine and operator, $\bar{p}_M$ is the average electrical power consumption, $t_M$ is the machining time, $C_{fix,M}$ is the fixed cost, and $C_{tl}$ is the tooling cost. In Eq. 16, $\bar{F}_t$ is the average tangential force, $r$ is the tool radius, and $\bar{p}_a(\Omega)$ is the average electrical power consumption for air cutting as a function of spindle speed. The average tangential cutting force and average start angle, $\bar{\phi}_s$, were calculated using Eqs. 17 and 18.

$$C_M = (r_{t,M} + \bar{p}_M r_e) t_M + C_{fix,M} + C_{tl} \quad (15)$$

$$\bar{p}_M = \bar{F}_t \Omega r + \bar{p}_a(\Omega) \quad (16)$$

$$\bar{F}_t = \frac{1}{\phi_e - \bar{\phi}_s} \int_{\bar{\phi}_s}^{\phi_e} (k_{tc} b f_t \sin\phi + k_{te} b) d\phi \quad (17)$$

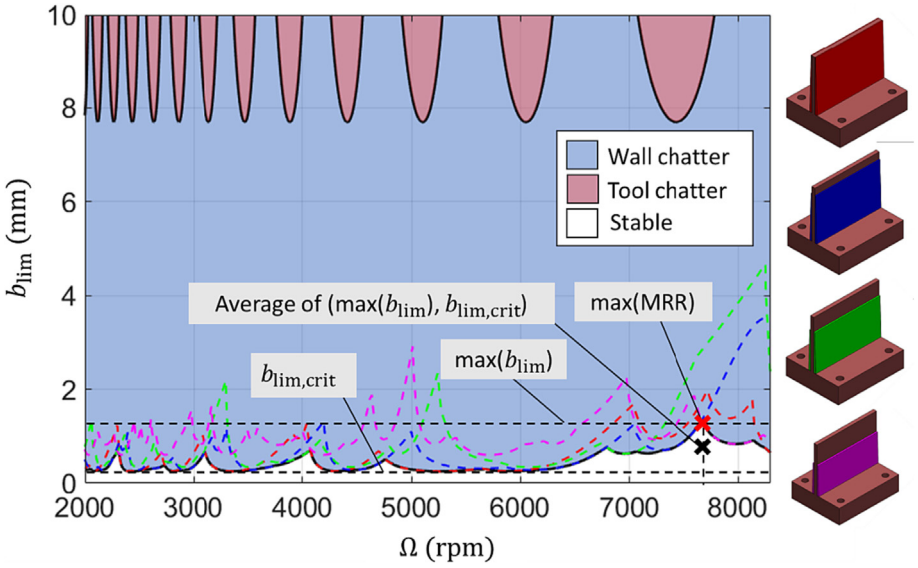


**Fig. 2.** Global stability map and selection of final spindle speed, Ω, and axial depth, $b$. The stability boundaries for multiple machining states of the wall (dashed lines) and the tool tip FRF are displayed.

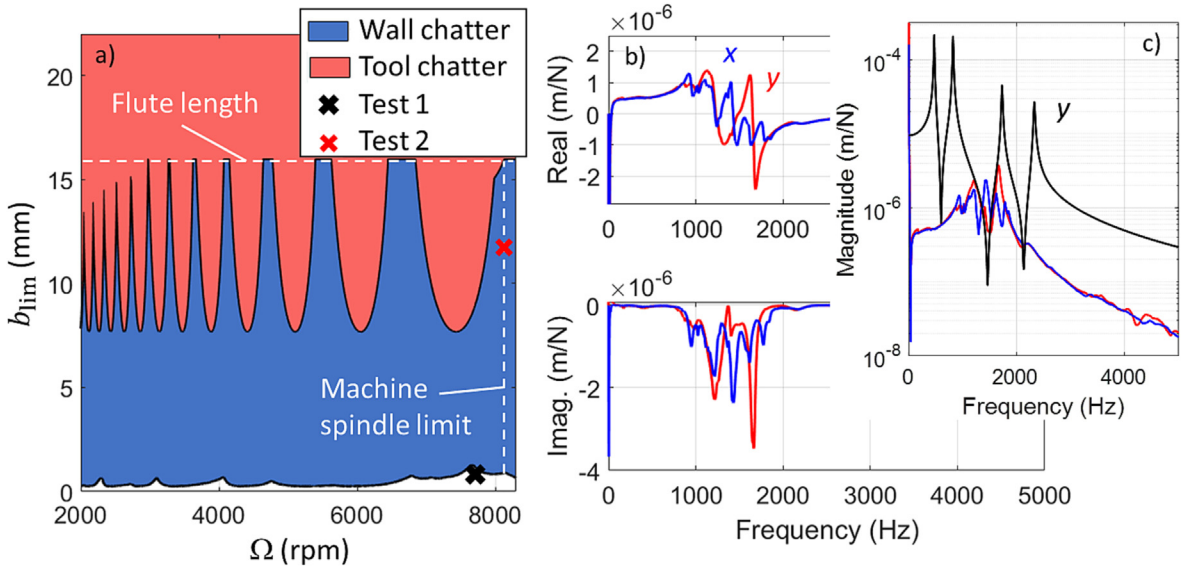


**Fig. 3.** (a) Stability map for $(t_1, t_2) = (1, 3)$ mm preform. (b) Tool tip FRFs in the $x$ and $y$ directions. (c) The inset displays the wall $y$ direction FRF (top center) magnitude superimposed on tool tip FRF magnitudes. A semi-logarithmic scale is used because the wall was more flexible in the tool for this example.

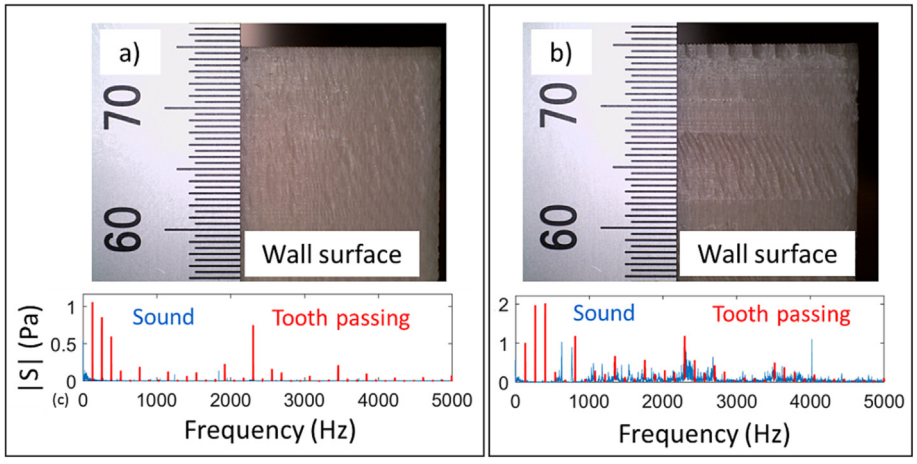


**Fig. 4.** (a) Test 1 results with wall surface finish and sound magnitude, |S|, vs. frequency. Stable behavior is observed. (b) Test 2 results with chatter.

$$\bar{\phi}_s = 180 - \cos^{-1}\left(1 - \frac{average(t_1, t_2)}{r}\right) \tag{18}$$

The machining process time was calculated as a function of the axial depth and feed rate, $f = \Omega N_t f_t$, for an integer number of axial passes. The tooling cost is described in Eq. 19, where $C_{pt}$ is the cost per tool, and $T$ is the tool life. A Taylor tool life model can be used to predict tool life, for example, which incorporates the cutting speed (spindle speed) and work material in the tool life calculation and, therefore, directly affects the tooling cost.

$$C_{tl} = C_{pt}\left(\frac{t_M}{T}\right) \tag{19}$$

## 5. Preform selection

To select a preform and corresponding machining parameters, the following values were used to populate Eqs. 11–19.

$r_m = 344,746.79/m^3$

$r_{t,AM} = 11.50/hr$

$C_{fix,AM} = 31.50$

$\bar{p}_{AM} = 9.2kW$

$f_t = 0.100mm$

$r_{t,M} = 200/\text{hr}$

$C_{tl} = 0;$ *negligible tool wear for ULTEM™ 9085*

$$\bar{p}_a(W) = \begin{cases} 0.22\Omega + 36.1 for \Omega < 6150 rpm \\ 0.45\Omega + 72.7 for \Omega \geq 6150 rpm \end{cases}$$

$r_e = 0.1445/kWh$

The AM, machining, and HM costs were calculated for each preform design. The minimum cost HM preform design was obtained for

$(t_1, t_2)$ = (1, 3) mm, while the highest cost was obtained for (5, 5) mm.

## 6. Experimental demonstration

Two machining experiments were conducted using the minimum cost preform $(t_1, t_2)$ = (1, 3) mm. The global stability map is displayed in Fig. 3, where stability boundaries are displayed for both the wall and tool. Because the tool was dynamically stiffer, its limit is higher than the combined wall limits (note that the wall limit changes with the $z$ location). Test 1 used an $(\Omega, b)$ combination that respected the limits imposed by both the tool and wall, while test 2 considered only the tool (i.e., rigid wall).

The machining setup included both a digital camera and unidirectional microphone to record video and audio during machining. The frequency content of the sound data was used to determine stability and the video was used to confirm machining time. Additionally, digital microscope images were collected for the machined surfaces.

Fig. 4 displays results for tests 1 and 2 from Fig. 3. For the test 1 $(\Omega, b)$ = (7678 rpm, 0.768 mm) combination, the cutting conditions were stable (i.e., frequency content is observed at the tooth passing frequency and harmonics) and no chatter marks are present on the machined surface; see Fig. 4a. For test 2 with $(\Omega, b)$ = (8100 rpm, 11.747 mm), on the other hand, fully developed chatter was observed. Fig. 4b shows chatter marks and frequency content at locations other than the tooth passing frequency and harmonics. This emphasizes the value of the new cost optimization framework for preform design, which incorporates the milling stability as a constraint.

## 7. Conclusions

This paper provided a new mathematical framework for optimum preform design in hybrid manufacturing. The framework selects the candidate design that gives the minimum combined cost for additive manufacturing (to produce the preform) and machining (to produce the required dimensions and surface finish). A novel contribution is constraint-based optimization, which respects the limiting depth of cut imposed by machining stability (i.e., machining parameters that produce chatter are rejected). A case study was included where a thin wall design was parameterized to describe the overbuilt deposition geometry. A grid of candidate solutions was selected using two wall thickness parameters. The cost and stability limit were calculated considering both the part and tool dynamics. The minimum cost option was deposited and machined to demonstrate the approach. Both stable and unstable machining parameters were selected to show the importance of including machining stability in the constrained optimization framework.

## Declaration of competing interest

The authors declare that they have no known competing financial interests or personal relationships that could have appeared to influence the work reported in this paper.

## Acknowledgements

This research was supported by the DOE Office of Energy Efficiency and Renewable Energy (EERE), Energy and Transportation Science Division, and used resources at the Manufacturing Demonstration Facility, a DOE EERE User Facility at Oak Ridge National Laboratory. This manuscript has been authored by UT-Battelle, LLC, under contract DE-AC05-00OR22725 with the US Department of Energy (DOE). The US government retains and the publisher, by accepting the article for publication, acknowledges that the US government retains a nonexclusive, paid-up, irrevocable, worldwide license to publish or reproduce the published form of this manuscript, or allow others to do so, for US government purposes. DOE will provide public access to these results of federally sponsored research in accordance with the DOE Public Access Plan (https://www.energy.gov/downloads/doe-public-access-plan). The authors also acknowledge support from the NSF Engineering Research Center for Hybrid Autonomous Manufacturing Moving from Evolution to Revolution (ERC-HAMMER) under Award Number EEC-2133630.

## References

[1] Bendsøe MP, Kikuchi N. Generating optimal topologies in structural design using a homogenization method. Comput Methods Appl Mech Eng 1988;71(2):197–224.
[2] Rozvany GI, Zhou M, Birker T. Generalized shape optimization without homogenization. Struct Optimiz 1992;4(3):250–2.
[3] Bendsøe MP, Sigmund O. Material interpolation schemes in topology optimization. Arch Appl Mech 1999;69(9):635–54.
[4] Eschenauer HA, Olhoff N. Topology optimization of continuum structures: A review. Appl Mech Rev 2001;54(4):331–90.
[5] Rozvany GI. A critical review of established methods of structural topology optimization. Struct Multidiscip Optim 2009;37(3):217–37.
[6] Sigmund O, Maute K. Topology optimization approaches. Struct Multidiscip Optim 2013;48(6):1031–55.
[7] Schmitz, T. and Smith, K.S., 2019. Machining Dynamics: Frequency Response to Improved Productivity, Second Edition. Springer, New York, NY.
[8] Tunc LT, Zatarain M. Stability optimal selection of stock shape and tool axis in finishing of thin-wall parts. CIRP Ann 2019;68(1):401–4.
[9] Smith S, Wilhelm R, Dutterer B, Cherukuri H, Goel G. Sacrificial structure preforms for thin part machining. CIRP Ann 2012;61(1):379–82.